Applied Catalysis B: Environmental 165 (2015) 149–157

Contents lists available at ScienceDirect

Applied Catalysis B: Environmental

journal homepage: www.elsevier.com/locate/apcatb

Nanotubes array electrodes by Pt evaporation: Half–cell characterization and PEM fuel cell demonstration

Samuele Galbiati[a], Arnaud Morin[a,*], Nicolas Pauc[b]

[a] LITEN-DEHT-Laboratoire des Composants pour Pile à combustible, Electrolyseur et Modélisation (LCPEM), CEA-Grenoble, 17 Rue des Martyrs, 38054 Grenoble Cedex 9, France
[b] INAC-SP2M-Silicium Nanoélectronique Photonique et Structures (SiNaPS), CEA-Grenoble, 17 Rue des Martyrs, 38054 Grenoble Cedex 9, France

ARTICLE INFO

Article history:
Received 6 August 2014
Received in revised form
26 September 2014
Accepted 30 September 2014
Available online 13 October 2014

Keywords:
Nanotubes array
Electron beam evaporation
PEMFC electrode
Fuel cell test
Catalyst activity

ABSTRACT

A self-standing nanotubes (NTs) array electrode is produced by electron beam evaporation of Pt on porous alumina templates. NTs have a mean diameter ranging from 150 to 300 nm, a length of 150 nm and a wall thickness of 20 nm. The ultrathin electrode has a density ranging between 10^9 and 4×10^9 NTs cm^{-2}_{geo} with a corresponding catalyst loading of 100 μg_{Pt} cm^{-2}_{geo}. The NTs are assembled on a Nafion® membrane to obtain a NTs Array based Membrane Electrode Assembly (NTA-MEA) for Polymer Electrolyte Membrane Fuel Cells (PEMFCs) application. Ex-situ half-cell tests are carried out on 0.5 cm^2_{geo} samples to characterize the electrochemical properties of the NTs array electrode. PEMFC tests are also performed on 17 cm^2_{geo} samples to demonstrate the great potential of this architecture as fuel cell cathode under real operating conditions. Comparisons with Pt/C dispersions are made to draw conclusions on the advantage of the NTs array on conventional electrodes in terms of catalyst utilization. The NTs array shows improved catalyst accessibility due to the absence of the porous carbon support. Double current density per catalyst unit surface over Pt/C dispersions is measured at 0.6 V during PEMFC tests under dry O_2 and air with 30%RH humidification.

1. Introduction

Conventional PEMFC electrodes are made of Pt nanoparticles dispersed in a porous carbon matrix (Pt/C) [1]. These systems show high active surface values (50–100 m^2/g_{Pt}) due to the small size of the dispersed catalyst particles (3– nm average size) [2], they are effective and easily adaptable to a large scale industrial production. In spite of this, several issues are still connected with this type of electrode. Pt nanoparticles show reduced surface specific activity towards the Oxygen Reduction Reaction (ORR) [3,4]. The durability of a Pt/C electrode is limited by the degradation of the carbon support and by the loss of Pt surface area through the potential-driven dissolution and agglomeration mechanisms [5–7]. The tortuosity of the active layer, related to the presence of the porous carbon support, induces strong limitations to the transport of reactants and products [8].

Huge effort has been recently addressed to the improvement of PEMFC catalyst layers, to overcome the previous issues and boost the ORR reaction at the cathode side. Several works focused on the development of new supports [9–14] and catalysts [15–17] to achieve higher stability and activity. Nevertheless substantial improvements can hardly be obtained by keeping carbon supported architectures, while they seem to be possible by adopting new self-supported nanostructures [18–23].

In particular self-supported catalyst nanotubes have been indicated as possible ways to approach the high catalyst surface activity of bulky Pt while getting rid of the porous carbon support. These features should eliminate the problems connected with the dissolution and agglomeration typical of dispersed catalyst nanoparticles. The absence of the carbon support should erase the carbon corrosion and should mitigate the mass transport limitations of reactants and products in the active layer.

Recent works have been carried out with the aim to electrochemically characterize the behavior of self-supported catalyst nanotubes [24–29]. These works mainly consist of ex-situ Rotating Disc Electrode (RDE) experiments during which a pure electrocatalyst is in direct contact with the acid electrolyte solution. In this experimental arrangement, nanotubes are usually dispersed without forming an ordered array and are not included in a real electrode structure.

Catalyst surface activity towards Oxygen Reduction Reaction (ORR) is usually evaluated at 0.9 V vs RHE. A 3–4 fold improvement

* Corresponding author. Tel.: +33 438785986.
E-mail address: arnaud.morin@cea.fr (A. Morin).

http://dx.doi.org/10.1016/j.apcatb.2014.09.075
0926-3373/

in surface activity over Pt/C dispersions is usually reported for these materials underlining excellent catalytic properties for such a kind of nanotubular structures.

In this frame RDE experiments are extremely useful to define the catalytic properties of a pure electrocatalyst, but they do not allow drawing conclusions on its behavior when part of a gas diffusion electrode assembled with a PFSA ionomer membrane. Furthermore, during PEMFC operation the catalyst is in direct contact with gas phase, the demanded current density is normally higher than during RDE experiments and the operating voltage is lower than 0.9 V.

Actually, when current is increasingly demanded, the operating point of a PEMFC shifts out of the active region of the polarization curve. In this situation, mass transport phenomena become progressively more important and the electrode mass transport losses might become predominant over the charge transfer losses. Testing catalyst nanotubes in a real electrode arrangement under conditions more similar to a real fuel cell operation would spread clarity on the effective benefit of this innovative support-free electrode structure. In this view, the test of directional arrays, instead of randomly dispersed nanotubes, is of particular interest since it might improve mass transport in the fuel cell active layer.

Directional electrode architectures have been successfully presented in the literature, where aligned arrays of carbon nanotubes have been successfully used as supporting catalyst structure [30,31]. This structure allows for a better utilization of the electrodes catalyst even though it keeps a carbon supporting structure.

In this work we present the production, the electrochemical half-cell characterization and the fuel cell test of an innovative membrane electrode assembly based on an array of self-supported Pt nanotubes.

The interest of such a new architecture as cathode of a fuel cell during real operation is demonstrated. Considerations about the advantage of the nanotubes array as fuel cell cathode in comparison to Pt/C dispersions in terms of catalyst utilization are drawn. To the authors' knowledge, the test of a Membrane Electrode Assembly based on an ordered Array of support-less catalyst Nanotubes (NTA-MEA) during PEMFC operation represents a novelty and helps in spreading clarity on the effectiveness of NTs for fuel cell energy conversion.

2. Experimental

2.1. Nanotubes array and MEA fabrication

The Pt-NTs array is produced by deposition of a controlled thin layer of Pt onto sacrificial templates of porous Anodic Aluminum Oxide (AAO, Anopore 47® by Whatman Ltd., diameter: 47 mm, thickness: 60 μm, average pore size: 200 nm) [32,33]. The deposition is carried out by Electron Beam Evaporation (EBE) using a commercial evaporator (MEB 550S, PLASSYS SA) by optimizing an available methodology [34]. During the deposition process, the AAO template is mounted on the rotating stage of the evaporator load lock chamber in face-down position. An energy intensive beam of electrons is directed towards the Pt target which is located in the evaporator's process chamber, below the AAO sample. The Pt target is consequently warmed up by the electron beam up to the evaporation temperature, Pt vapors are therefore released and redeposit on the rotating AAO template. The process takes place under vacuum pressure ($1{,}5 \times 10^{-6}$ Torr) and the Pt vapors are therefore collimated. The rotating speed of the turning stage was $15^{\circ}\,s^{-1}$ and the incidence angle between the collimated Pt vapors and the AAO sample was set at 45° by tilting the rotating stage. A Pt amount of 75 nm estimated on a horizontal surface is evaporated with a speed rate of 0.25 nm s^{-1}. This resulted in a 20 nm thick Pt layer on the tilted surface of the porous AAO layer, which corresponds to a loading of 100 $\mu g_{Pt}\,cm^{-2}{}_{geo}$.

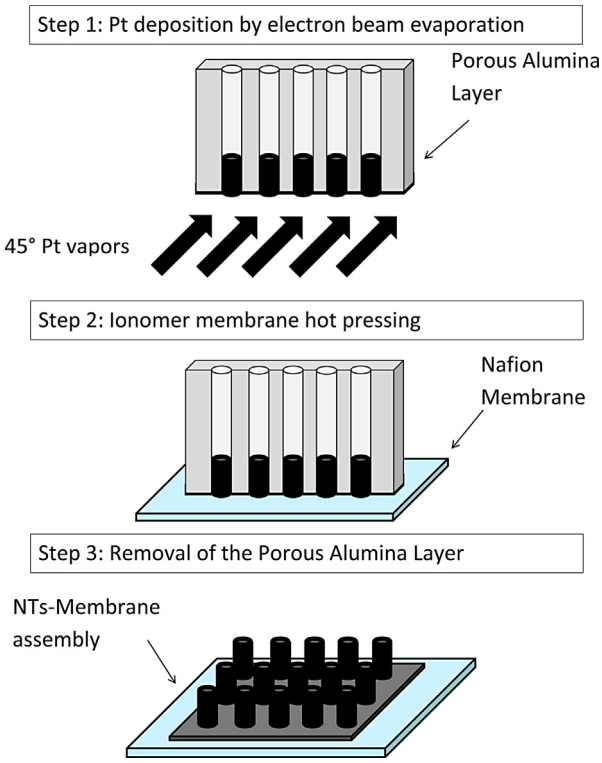

Fig. 1. Schematic drawing of the 3 steps fabrication process of the NTs array based membrane electrode assembly (NTA-MEA).

The Pt coated AAO template was stuck onto a Nafion® HP membrane (thickness: 20 μm) by hot pressing at 135 °C for 10 min with a pressure of 340 N cm^{-2}, by putting the Pt-covered side in contact with the polymer layer. This step allows achieving a full adhesion of the AAO sample onto the membrane. After hot pressing, the AAO/Nafion® membrane assembly is immersed into NaOH [1 M] for 1 h to dissolve the AAO template. As a consequence, an array of free-standing Pt NTs is left on the Nafion® electrolyte membrane forming a NTs array based Membrane Electrode Assembly (NTA-MEA) for PEMFC use. After fabrication, the NTA-MEA is rinsed in ultrapure water (Millipore® grade) to wash away possible impurities resulting from the AAO etching. The assembly is subsequently immersed into HNO_3 [1 M] for 1 h in order to re-acidify the membrane and to remove any eventual metallic cations and organic impurities. A new cleaning in ultrapure water (Millipore® grade) is finally done. This straightforward template-based methodology is schematically shown in Fig. 1 and allows obtaining nanotubes based MEAs in a fast and reproducible way. The adhesion of the NTs array electrode on the Nafion® membrane is excellent and the resulting NTA-MEA is ultrathin, flexible and includes no carbon support.

2.2. Pt/C dispersion electrodes fabrication

Two conventional Pt/C supported electrodes were fabricated in order to make comparisons with the NTs array electrode. The first electrode (hereon named Pt/C-SE electrode) was fabricated by spraying a catalyst ink (Tanaka 50 wt% onto Vulcan XC72) on a SGL-24BC gas diffusion layer support. The spraying was optimized by subsequent tries until the same ECSA of the NTs array electrode was obtained. The final loading of the Pt/C-SE electrode is 20 $\mu g_{Pt}\,cm^{-2}{}_{geo}$, the average active layer thickness is less than 1 μm (cross section view available in Fig. S1(a) in the supplementary

data). The second electrode (hereon named Pt/C-STD electrode) was fabricated by screen printing [35] in the pilot plant of the fuel cell components laboratory of CEA-Grenoble. The Pt/C-STD electrode is also based on the same commercial catalyst ink (Tanaka 50 wt% onto Vulcan XC72) and is supported on a SGL-24BC gas diffusion layer. The Pt loading of this electrode is 170 $\mu g_{Pt}\,cm^{-2}{}_{geo}$, the average active layer thickness is around 7 μm (cross section view in Fig. S1(b) of the supplementary data). The comparison of the NTs array electrode with the Pt/C-SE electrode provides information on the exploitation of the same catalyst surface in the shape of bulky Pt-NTs or of carbon supported Pt nanoparticles. The comparison with the Pt/C-STD electrode is made to contrast the innovative Pt-NTs array electrode with a conventional benchmark Pt/C electrode.

2.3. Half-cell experiments

The electrochemical properties of the NTs array electrode were investigated during half-cell experiments at ambient temperature and pressure in a nitrogen saturated H_2SO_4 solution (0.5 M) [36,37]. A scheme of the half-cell experimental setup is provided in Fig. S2 of the supplementary information. A Mercury Sulphate Electrode (MSE) and a Pt grid were immersed in the acid bath to work as reference (RE) and counter electrode (CE), respectively. The NTs array (Working Electrode, WE) is in direct contact with the dry gas phase by a gas diffusion layer (SGL 24 BC), while the acid solution is separate by the electrolyte membrane. Current is collected by means of a gold grid and is recorded by a potentiostat (BioLogic VMP2). Cyclic Voltammetry was measured under N_2, H_2, O_2 and CO [50 ppm in H_2] at a speed rate of 20 mV s^{-1} with a constant dry gas flow of 60 N ml min^{-1}. Electrochemically Active Surface (ECSA), ORR activity, CO poisoning velocity, CO stripping area and electrolyte resistivity were determined on 0.5 cm^2 samples. Values with reference to MSE electrode were reconverted and displayed with reference to Reversible Hydrogen Electrode (RHE). More experimental details concerning electrochemical half-cell experiments are reported in the supplementary information.

2.4. Fuel cell assembly

A fuel cell was assembled with the nanotubes array electrode facing the cathode flow field (Figure S3 in the supplementary data), a SGL-24BC gas diffusion layer was applied on the nanotubes array electrode. MEAs were also assembled with the Pt/C-SE and the Pt/C-STD as cathode electrodes. The same conventional Pt/C electrode (Tanaka 50 wt% onto Vulcan XC72, loading: 200 $\mu g_{Pt}\,cm^{-2}{}_{geo}$) is used as anode for all of the assembled MEAs.

When nanotubes array electrodes are tested, the MEA geometrical active area is 17 cm^2 which corresponds to the geometrical area of the AAO template used for the electrode fabrication (47 mm in diameter). Conversely, when Pt/C electrodes are tested, the MEA active area is 25 cm^2. Graphite flow fields with a single serpentine path (1.4 mm × 1.4 mm square section) are used on both the anode and the cathode side. Stainless steel plates provided with thermal resistances are used to hold the assembly and to heat up the cell. A tailored gaskets system is applied to tighten the fuel cell.

2.5. Fuel cell testing

Fuel cell tests are carried out by measuring polarization curves using a BioLogic FCT 50S fuel cell test bench. Polarization curves are measured by scanning the fuel cell current with a speed of 0.16 mA s^{-1}, while voltage is recorded as response. Pure hydrogen ($\lambda_{H2} = 1.2$) is sent to the anode side while pure oxygen ($\lambda_{O2} = 1.5$) and air ($\lambda_{Air} = 2$) are alternatively tested on the cathode side. Minimum gas flows are 50 N ml min^{-1} for both the anode and cathode streams. Reactants streams are externally humidified to achieve 30%, 50% and 100% relative humidity (RH). Experiments with dry reactants are also performed by bypassing the humidification system. Both the anode and the cathode compartments are pressurized at 0.5 bar relative by adjusting a backpressure regulation system. The temperature of the cell is set at 80 °C throughout the whole experimental activity. Tubings and connecting manifolds are heated at 85 °C to prevent water condensation. A potentiostat (BioLogic VSP) combined with a booster (BioLogic VMP2B) was periodically connected to measure electrochemical impedance spectra (EIS) and cyclic voltammetry (CV). In this last case pure nitrogen (50 N ml min^{-1}) instead of air is fed to the cathode compartment. Before starting the test of a nanotubes array based MEA, voltage is cycled at 50 mV s^{-1} under H_2 and N_2 in order to clean the catalyst surface. Voltage cycling is continued until the voltammograms reach a stable profile.

2.6. Scanning Electron Microscope analysis

The structure of the nanotubes array electrodes is investigated by microscope observation using a LEO Gemini 1530 Scanning Electron Microscope (SEM) available at the "Minatec" microscopy facility of CEA-Grenoble. The microscope was operated at 5 kV and In-Lens detectors were used for the acquisition of images.

2.7. Catalyst loading determination

The Pt loading of the electrodes is measured by UV spectrometry. MEA samples are initially heat treated in a ceramic oven at 600 °C for 15 h so that all the components of the other than Pt are oxidized and vented out of the furnace. The remaining Pt catalyst powder is chemically treated to convert it to the Pt^{4+} ionic form, which is needed to perform the UV measurements. The treatment consists in the dilution of the Pt catalyst powder in a solution of 25%vol HNO_3 and 75% vol HCl (Aqua Regia). The solution is completely evaporated at 120 °C into a dedicated glass system. This step is repeated other two times with concentrated HCl [12 M]. The obtained dry catalyst is finally diluted in HCl [1 M] where the Pt^{4+} ions are stable. The obtained solution is analyzed to determine the catalyst concentration by using a UV spectrometer (Shimadzu 1800). A calibration of the UV spectrometer is made before each measurement by using reference samples.

3. Results and discussion

3.1. Electrode structure

SEM pictures of the free-standing Pt NTs array electrode are shown in Fig. 2. Fig. 2a and b show the top and cross sectional view of the Pt-coated side of the AAO template which is in contact with the Nafion® membrane during the hot pressing. These images indicate that, after the Pt coating, the porosities of the AAO template are still open. Therefore nanotubes have open tips and basis, and a thin Pt layer is left only between subsequent tubes, which allows interconnecting the array. This layer might alter the transport of water from cathode and anode and of the protons from anode to cathode. After all the steps of the fabrication process, the NTs array is extremely uniform and regular. The mean internal diameter of the NTs is around 150 nm if the Pt coating takes place on the branched side of the AAO template (Fig. 2c), while it is around 300 nm on the regular side (Fig. 2d). The resulting arrays of Pt-NTs have a density of approximately 4×10^9 NTs $cm^{-2}{}_{geo}$ and 1×10^9 NTs $cm^{-2}{}_{geo}$ if the Pt deposition takes place on the branched or on the regular side of the AAO template, respectively. The surface of the electrode is clean and no collapsed nanoparticles or impurities are present. The thickness of the nanotubes walls approaches 20 nm (Fig. 2e), the walls are consistent and stiff, and the nanotubes are self-standing. The

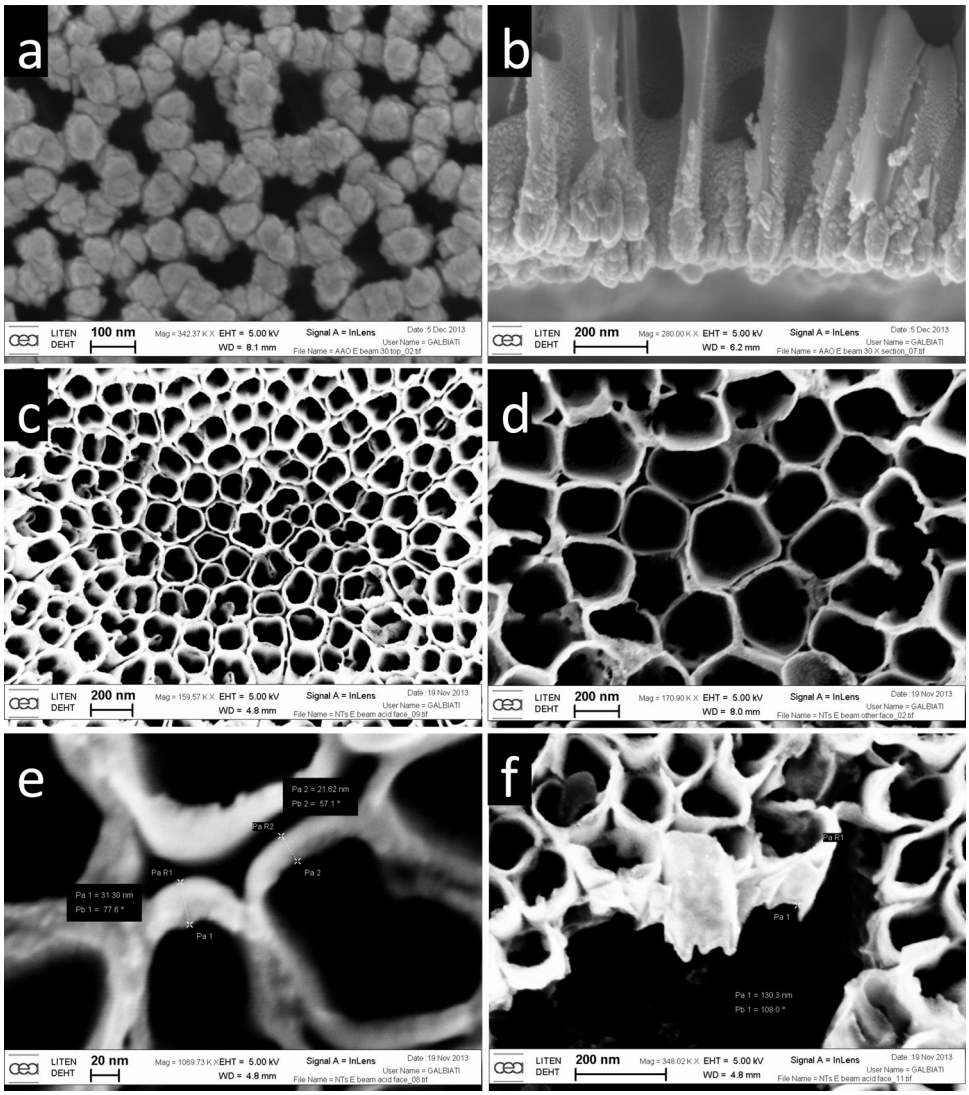

Fig. 2. (a) Top view of the AAO template after Pt deposition showing open porosities; (b) Cross section of the AAO template after Pt deposition. (c) Top view of the NTs array obtained by coating the branched side of the AAO template; (d) Top view of the NTs array obtained by coating the regular side of the AAO template; (e) Enlarged view of the top of the NTs array showing the 20 nm thick Pt layer; (f) Tilted view of the NTs array showing the height of the tubes included between 150 nm and 200 nm.

top of the single nanotube is open and the internal surface is accessible by the gaseous reactants. The length of the NTs is included between 150 and 200 nm (Fig. 2f). Such a limit is due to the stage tilting angle of 45° with respect to the Pt vapors direction during the electron beam deposition process [34]. Due to their shortness, nanotubes are straight and do not collapse, no agglomeration or packing takes place as it frequently happens when longer tubular structures are produced [38,39].

The final Pt loading of this electrode architecture is as low as 100 $\mu g_{Pt}\ cm^{-2}{}_{geo}$, as determined by UV spectrometry.

3.2. Half-cell electrochemical characterization

3.2.1. Electrochemically active surface area

The NTs array was characterized during half-cell experiments (technique explained in Section 2.3) and it was compared with the two Pt/C electrodes described at Section 2.2. The electrochemically active area, the CO poisoning trend and the CO stripping area were measured by cyclic voltammetry (CV) under dry N_2 and CO [50 ppm in H_2]. The related graphs are shown in Fig. 3a,b and c respectively while the characteristics of the investigated electrodes are summarized in Table 1.

The ECSA of the NTs array electrode is around 17 $cm^2{}_{Pt}\ cm^{-2}{}_{geo}$, which is a rather small value if compared to the ECSA obtainable with longer nanotubes [38]. A comparable ECSA (19 $cm^2{}_{Pt}\ cm^{-2}{}_{geo}$) was measured on the Pt/C-SE electrode which was produced with a Pt loading of 20 $\mu g_{Pt}\ cm^{-2}{}_{geo}$, 5 times lower than the loading of the NTs array electrode. The Pt/C-STD electrode exhibits an ECSA of 110 $cm^2{}_{Pt}\ cm^{-2}{}_{geo}$ which is approximately 6 times larger than

Table 1
Properties of the NTs array electrode, of the Pt/C-SE and of the Pt/C-STD dispersion electrodes. Active areas were measured by Cyclic Voltammetry during half-cell experiments. Pt loading was measured by UV spectrometry. Catalyst geometrical area was estimated under the hypothesis of perfectly cylindrical nanotubes with smooth walls fort he NTs array electrode, and spherical Pt nanoparticles with a diameter of 4 nm for the Pt/C electrodes.

	NTs array	Pt/C-SE	Pt/C-STD
Pt loading [$\mu g_{Pt}\ cm^{-2}{}_{geo}$]	100	20	170
Geometrical area [$cm^2{}_{Pt}\ cm^{-2}{}_{geo}$]	12	20	158
ECSA under N_2 [$cm^2{}_{Pt}\ cm^{-2}{}_{geo}$]	17	19	110
ECSA/Geo area [%]	140	95	70
CO stripping area/ECSA [%]	100	100	70
CO poisoning time	15 min	90 min	>3 h
Poisoning rate [$min\ cm^{-2}{}_{Pt}$]	0,8	5	>2

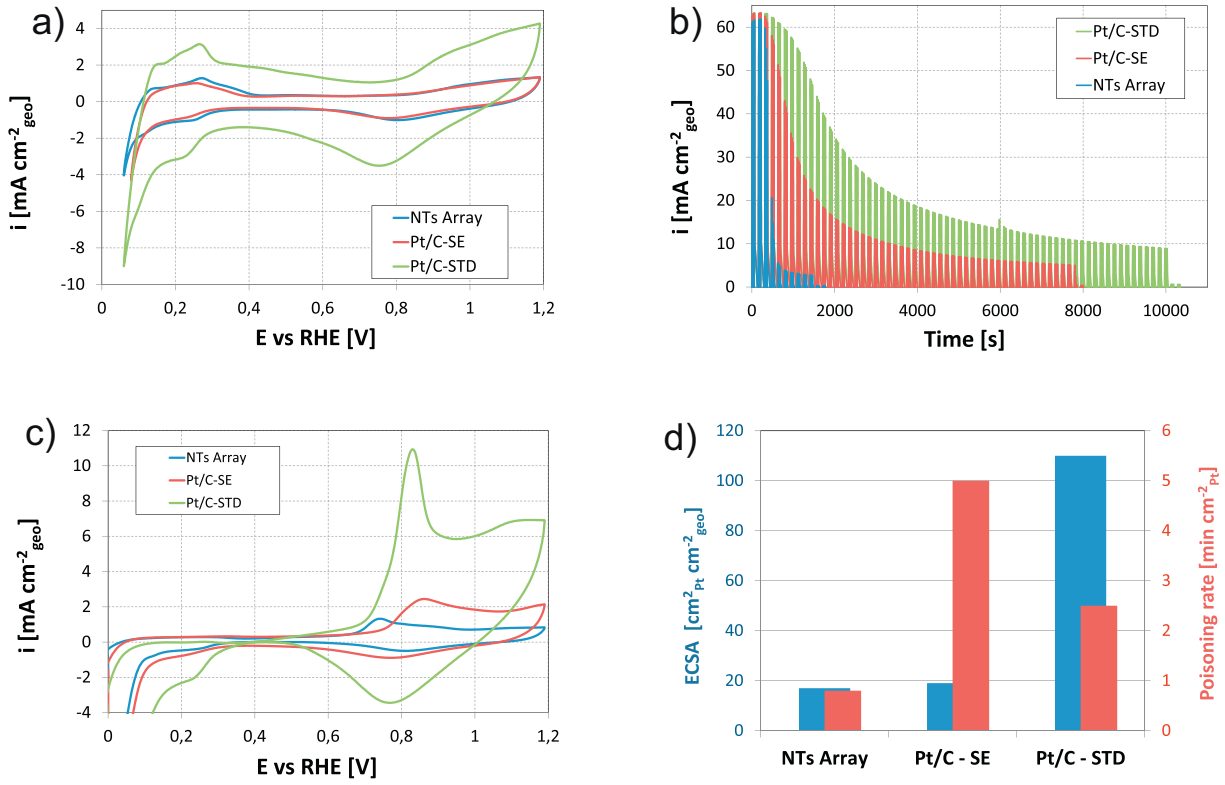

Fig. 3. (a) Cyclic voltammograms under N_2, (b) CO poisoning voltammograms, (c) CO stripping voltammograms, d) ECSA and poisoning rate, measured in half-cell setup for the NTs array, the Pt/C-SE and the Pt/C-STD electrodes. Poisoning rate is defined as the ratio between CO poisoning time and CO stripping area.

the one of the NTs array and Pt/C-SE electrodes, while its Pt loading is 1.7 and 8.5 times higher respectively. Pt/C dispersions exhibit high ECSA values in comparison to bulky Pt-NTs structures due to the high specific surface of the finely dispersed Pt nanoparticles. Nevertheless, their ECSA does not increase linearly with the Pt loading. Actually, due to the increasing thickness of the active layer, a progressively larger number of dispersed Pt nanoparticles is not included in the triple phase contact [40].

In spite of its limited value, the active surface of the NTs is fully active and the measured ECSA corresponds to 140% of the geometrical surface. On the other side, the ECSAs of the Pt/C dispersions correspond to 95% (Pt/C-SE) and 70% (PT/C-STD) of the estimated geometrical area values.

The 140% surface utilization of the NTs array electrode is due to the roughness of the Pt walls of the NTs, which confers higher surface than calculated under the hypothesis of perfectly smooth Pt walls [24,38]. The whole internal and external surface of the NTs is available for proton transport even though no Nafion® or proton conducting material was coated on their surface. Such a fact is attributed to the thinness of the electrode and to its good hydration during half-cell experiments. Differently, the ECSA of the Pt/C electrodes derives from the presence of the triple phase contact between the Pt nanoparticle, the proton conducting material and the electron conducting material in the electrode. Such a value is limited below 100% and decreases as the loading increases due to the thicker active layer and harder control on the electrode structure. The Pt/C-SE electrode shows a high value of catalyst surface utilization (95%), due to its low loading and thin structure. Such a value decreases down to 70% for the Pt/C-STD electrode due to the higher loading and consequently thicker active layer. As a consequence, in this benchmark electrode around 30% of the catalyst active surface is not used.

CO stripping experiments [41] were carried out after a preliminary poisoning period under CO [50 ppm in H_2]; voltammograms for the three investigated electrodes are shown in Fig. 3c. The CO stripping peak of the NTs array electrode is shifted to lower potential (0.73 V vs RHE) if compared to the Pt/C electrodes (0.83 V and 0.85 V vs RHE for the Pt/C-STD and the Pt/C-SE electrodes respectively). The same behavior has been observed in other studies on Pt NTs [24,38] and underlines that a lower potential is sufficient to oxidize CO, similarly to what happens with bulky Pt. The CO stripping area values (Table 1) measured on the NTs array and on the Pt/C-SE electrodes equal the corresponding ECSA measured under N_2. Differently, the CO stripping area of the Pt/C-STD electrode is only 70% of the corresponding ECSA. This means that, for the first two electrodes the whole ECSA is also contactable by the gas phase, while, for the last electrode, around 30% of the ECSA is not accessible by the gaseous reactants and it is therefore not used. Such a difference is explained by the presence of a thicker porous carbon layer which hinders the gas transport to some of the active sites. In this structure, part of the Pt active surface is not contacted by the gas species and is therefore not active [40–43]. Such a negative effect is not present in the NTs array due to the absence of the C support and it is negligible in the Pt/C-SE electrode due to the low loading and limited thickness. The negative effect of the carbon supporting structure is also pointed out by CO poisoning experiments [38], which are graphically shown in Fig. 3b. The poisoning of the NTs array electrode happens much faster than the one of the Pt/C-SE, which is provided with the same ECSA. Actually in the first case the time required to poison 90% of the catalyst surface is around 15 min while in the second case it rises up to around 90 min underlining a more difficult gas path to the catalyst active sites. Such a time becomes longer than 3 h for the Pt/C-STD electrode. The ECSA and the surface-normalized poisoning times are shown in Fig. 3d. The poisoning times are not proportional to the poisoned catalyst surface and indicate easier gas transport and catalyst exposition in the NTs architecture over both of the Pt/C dispersions, due to the absence of the porous carbon support.

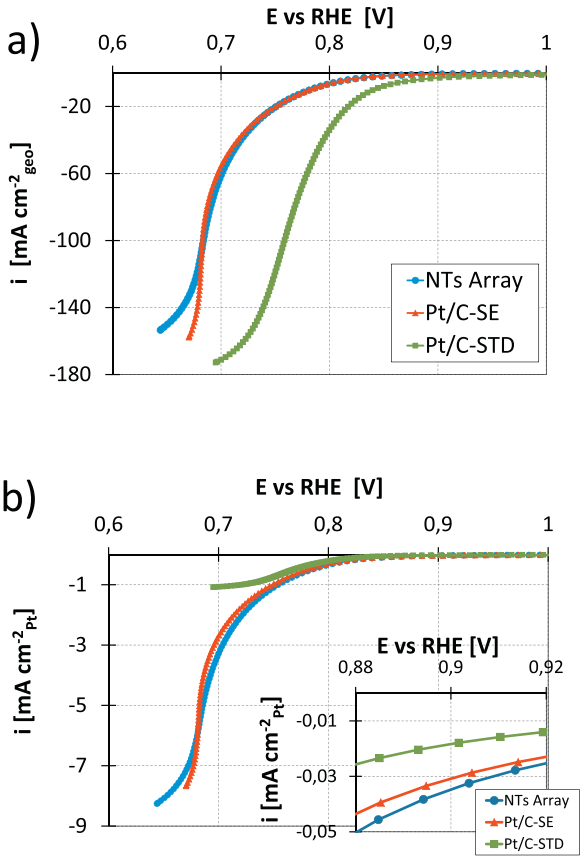

Fig. 4. ORR curves measured during half-cell experiments under O_2 with reference to the electrode unit area (a) and to the catalyst unit area (b).

3.2.2. ORR activity

Fig. 4a shows the ORR curves measured in half-cell setup under pure dry O_2 for the NTs array and the Pt/C-SE and Pt/C-STD dispersion electrodes.

This plot refers to the specific current density per electrode geometrical unit area. The NTs array and the Pt/C-SE electrode exhibit similar i/V trends and no consistent difference can be noticed. This finding indicates that, during half-cell experiments, the catalyst surface behaves in the same way in the form of bulky NTs or dispersed Pt nanoparticles without any influence due to the different catalyst structure. On the other side, the Pt/C-STD dispersion electrode exhibits much higher current density for a given voltage value over the previous electrodes. This finding is due to the much larger ECSA of this electrode and indicates better performance on a geometrical basis. Fig. 4b shows the ORR curves with respect to the catalyst unit surface, these curves were obtained by dividing the electrode geometrical current density by the electrodes ECSAs. On a catalyst surface specific basis, the NTs array electrode and the Pt/C-SE electrodes show the best performance and reach current density higher than the Pt/C-STD electrode. The first two electrodes can deliver a current density as high as 8 mA $cm^{-2}{}_{Pt}$ with a flat profile, while the Pt/C-STD electrode undergoes a sharp voltage drop which limits its current density below 1 mA $cm^{-2}{}_{Pt}$.

These current density values are inferior to the current density which is normally achieved in a PEMFC during operation. Such a fact is mainly due to the huge total resistance of the electrolytic bath and to the abundant hydration of the electrode in the half-cell setup. The direct contact of the Nafion® electrolyte membrane with the acid solution might induce a nearly flooded condition, thus limiting the electrodes maximum current yield. The half-cell test points out a huge difference in the behavior of the electrodes and underlines that the NTs array and the Pt/C-SE dispersion with equivalent ECSA offer better mass transport properties and allow reaching higher current density per catalyst unit area, in spite of the nearly flooded condition. On the other side, the extremely low current density per catalyst unit area obtained by the Pt/C-STD dispersion electrode is attributed to the thicker porous carbon layer which limits the gas transport to the Pt active sites, as already indicated by the CO poisoning experiment. Therefore, the Pt/C-STD electrode is capable of delivering high performance on an electrode geometrical basis due to its large ECSA, but it exhibits extremely poor exploitation of the available Pt surface.

The absence of the porous carbon layer in the NTs array eliminates the problem related to the accessibility of the catalyst surface, which is completely contactable by the reactants. The Pt/C-SE electrode also shows good gas accessibility due to the thin active layer, but in this case mass transport issues would increase with the loading when looking for larger ECSA and higher power density, as it happens with the Pt/C-STD electrode. This effect is not present in the NTs array, where the catalyst surface would be always directly exposed to reactants, even when larger ECSAs are pursued. As obtained by the performed half-cell experiments, the advantage of the Pt NTs array consists of the better catalyst accessibility and mass transport properties while the catalyst surface activity remains the same as in the Pt/C-SE dispersion electrode. The real limitation of NTs arrays stands in the limited Pt mass specific ECSA which is around 5 times lower than for Pt/C dispersions [28]. If larger active areas can be achieved reducing the Pt amount and keeping the same catalyst surface accessibility and utilization, NTs arrays might become competitive with Pt/C electrodes. According to our calculations, this gap could be recovered by producing arrays with a density of 10^9 NTs $cm^{-2}{}_{geo}$, with a mean NTs diameter of 250 nm, a length of around 7 μm and 5 nm thick walls. In this case Pt walls would be made by interconnected nanoparticles, which deliver the smallest possible wall thickness [24,27,44].

Due to the effect of porosity and roughness, the ECSA of the NTs array would be 40% to 100% larger than geometrical. In such a situation, NTs array electrodes with an ECSA of 200 $cm^2{}_{Pt}$ $cm^{-2}{}_{geo}$ and a loading around 350 μg_{Pt} $cm^{-2}{}_{geo}$ could be fabricated. In this perspective, mass specific ECSAs comparable to the ones of Pt/C dispersions could be obtained, by preserving the advantages of the NTs array architecture in terms of mass transport and catalyst accessibility.

3.3. Fuel cell test

A complete MEA was assembled with the NTs array electrode on the cathode side (active surface: 17 $cm^2{}_{geo}$, shown in Figure S3 in the supplementary information) and with a conventional Pt/C dispersion on the anode side (Tanaka 50% wt on Vulcan XC72, Pt loading: 200 μg_{Pt} $cm^{-2}{}_{geo}$). The NTs array based MEA (NTA-MEA) was tested in a fuel cell assembly at 80 °C and polarization curves were recorded feeding pure H_2 to the anode and air to the cathode with stoichiometric regulation. Reactants were externally humidified at 30%, 50% and 100% RH before entering the fuel cell structure, the same humidification rate was applied simultaneously to the anode and cathode streams. Tests under dry H_2/air and dry H_2/O_2 were also performed.

The same fuel cell test was carried out on MEAs assembled with the Pt/C-SE and Pt/C-STD electrodes as cathodes (hereon named Pt/C-SE-MEA and Pt/C-STD-MEA respectively). All of the assembled MEAs were provided with the same type of anode electrode in order to eliminate any effect due to the anode structure, thus creating a direct connection between the fuel cell performance and the cathode electrode structure. Such a comparison allows spreading clarity

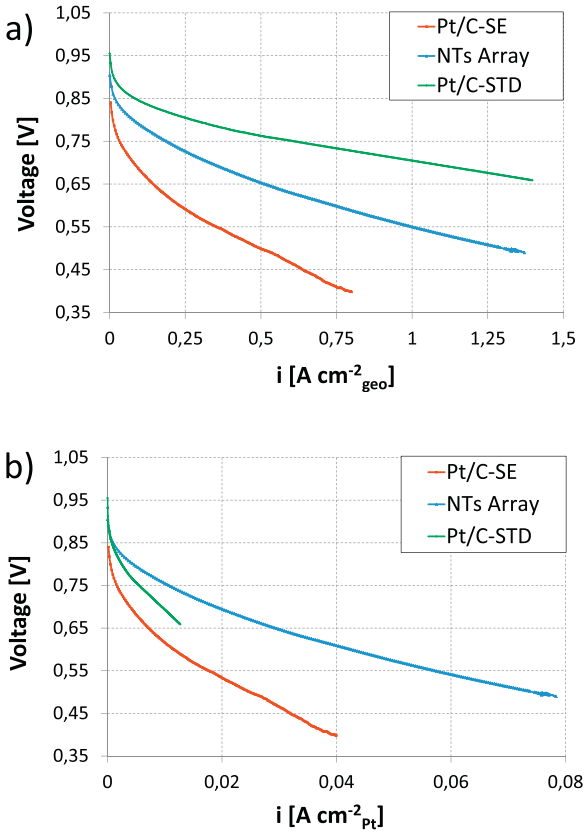

Fig. 5. Fuel Cell polarization curves under dry H_2/O_2 with reference to the electrode unit surface (a) and to the catalyst unit surface (b).

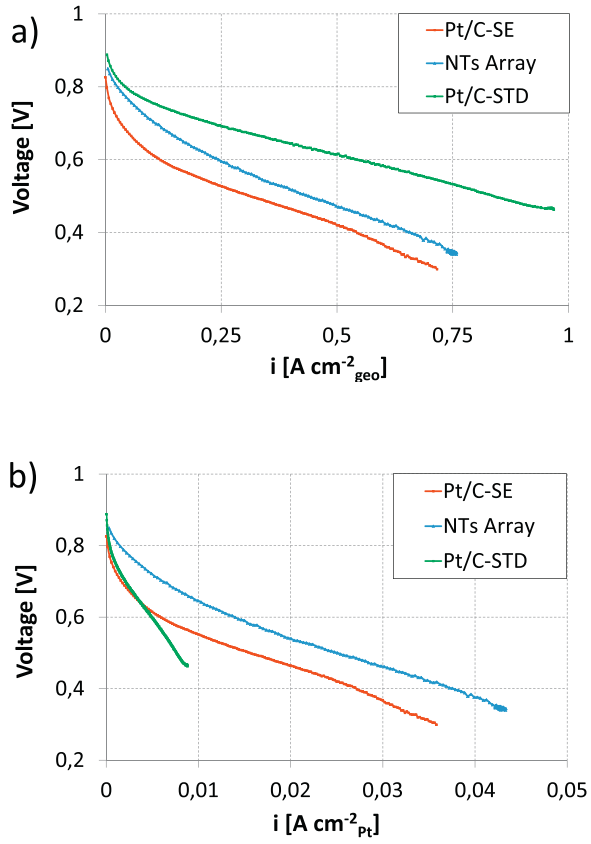

Fig. 6. Fuel Cell polarization curves under H_2/Air at 30% RH with reference to the electrode unit surface (a) and to the catalyst unit surface (b).

on the properties of the NTs array electrode in comparison with the Pt/C dispersions during real PEMFC operation.

3.3.1. Operation under dry H_2/O_2

Fig. 5a shows the polarization curves recorded under dry H_2/O_2 for the NTA-MEA and for the Pt/C-SE-MEA and the Pt/C-STD-MEA respectively.

The polarization curves are reported as function of current density per electrode unit area. The Open Circuit Voltage (OCV) is around 0.95 V for both the NTs array and the Pt/C-SE electrodes. Thus, there is no evidence of cross-over that could be due to damage of the membrane by the NTs array. The integrity of the membrane seems to be preserved after all the steps of the fabrication process of the NT array. The NTA-MEA shows better performance than the Pt/C-SE-MEA, this means that in a complete PEMFC operated under dry H_2/O_2, the same Pt active surface performs better under the shape of bulky nanotubes than Pt nanoparticles dispersed on a C support. Such an improvement was not visible during half-cell experiments, where the two electrodes exhibited the same activity towards ORR. The improvement during PEMFC operation under dry H_2/O_2 is therefore ascribed to the better mass transport to and from the catalyst active surface which takes place in the NTs electrode, in relation to a Pt/C electrode provided with the same ECSA.

On the other side, the Pt/C-STD-MEA has higher performance per electrode unit area than the NTA-MEA. This is due to the larger ECSA of the Pt/C-STD electrode which compensates the disadvantage of its thicker porous carbon support. Fig. 5b shows the polarization curves under dry H_2/O_2 as a function of current density per catalyst unit area. On a catalyst specific basis, the NTA-MEA exhibits the best performance which corresponds to the best Pt surface exploitation in comparison to both of the tested Pt/C cathode dispersions. This finding indicates that in the NTs array structure, the Pt unit surface is used in a more efficient way than in Pt/C dispersions. In such an array, higher current density per Pt surface unit can be drawn with a higher voltage profile. The improvement in Pt surface exploitation is consistent and it is due to the enhanced gas accessibility of the Pt NTs structure, which is possible due to the absence of the porous C support. The NTs array delivers improved Pt surface utilization even over state of the art Pt/C dispersions also during in-situ PEMFC operation.

3.3.2. Operation under 30%RH humidified H_2/Air

Polarization curves have been recorded with 30%RH humidified H_2/air, which represents a condition of practical interest for real fuel cell systems. 30%RH is the optimal humidification rate for the NTA-MEA, as obtained by a sensitivity analysis on this electrode architecture (Fig. S4 in the supplementary information). Despite the absence of ionomer, NTs require an inferior humidification rate in comparison to both the Pt/C-SE and the Pt/C-STD electrodes which achieve maximum performance under fully humidified conditions (Figs. S5 and S6 in the supplementary information).

The polarization curves are plot with relation to the electrode unit area (Fig. 6a) and to the catalyst unit area (Fig. 6b).

Considering the electrode unit area, the polarization curve of the NTs array MEA is once again better than the one measured with the Pt/C-SE electrode. This trend is coherent with the one measured under dry O_2, even though, under humidified air, the improvement is less pronounced. With the same reference to the electrode unit area, the Pt/C-STD electrode still exhibits the highest performance due to its high ECSA, as it was also observed under O_2.

This evidence supports the effectiveness of the standard Pt/C-STD dispersion in order to obtain high performance per electrode unit surface. On the other side, by considering the Pt catalyst unit area (Fig. 6b), the performance of the NTA-MEA is once again

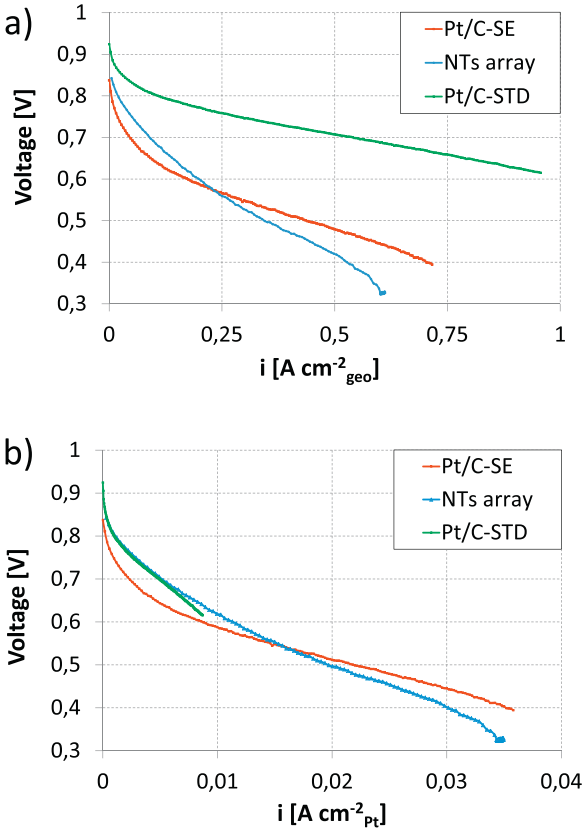

Fig. 7. Fuel Cell polarization curves under H_2/Air at 100% RH with reference to the electrode unit surface (a) and to the catalyst unit surface (b).

superior to the one of both the Pt/C-SE and the Pt/C-STD electrodes. This confirms for the improved catalyst surface exploitation of this innovative electrode architecture in comparison to conventional Pt/C electrodes, also under H_2/air feed streams at 30%RH humidification.

3.3.3. Operation under fully humidified H_2/Air

Fig. 7a shows the polarization curves measured on the three considered MEAs under fully humidified reactants (H_2/Air), with reference to the electrode unit area.

During operation under fully humidified conditions, the advantage provided by the NTs becomes less consistent. The maximum achievable current density per electrode unit area decreases with respect to the operation under dry O_2 and Air at 30%RH humidification. The polarization curve of the NTA-MEA approaches the one of the Pt/C-SE-MEA, as it was observed during half-cell experiments. The voltage drop becomes sharper as current density increases, which can be ascribed to water management issues related to the excessive electrode hydration.

The same behaviour can be observed also when the catalyst unit area is considered (Fig. 7b). In this case, at current density lower than 0.01 A $cm^{-2}{}_{Pt}$, the polarization curve of the NTA-MEA equals the one of the benchmark Pt/C-STD-MEA. Conversely, at current density higher than 0.01 A $cm^{-2}{}_{Pt}$, voltage drops gradually below the one of the Pt/C-SE-MEA. The operation of the NTs array under fully humidified reactants is therefore critical, especially at high current density, due to water management issues [37]. Such a fact is ascribed to the presence of extra water that might hinder the transport of reactants when high current density is demanded. In spite of this, even in this disadvantageous condition, the specific performance of the nanotubes array per catalyst unit area is similar to the one of the Pt/C dispersion electrodes when the voltage range is included between 0.6 V and 0.7 V, which corresponds to the real operating voltage range of a PEMFC. As already stated above, the NTs array electrode exhibits the best performance using air at 30%RH, and increasing the reactants humidification is detrimental, but it is interesting to notice that the electrode can operate satisfactorily with fully humidified gases because no dramatic flooding occurs. This behaviour is very different from the one of Pt/C dispersions, which show maximum performance at 100%RH reactants humidification. This represents a huge advantage when running a real fuel cell system since it would turn into a modest reactants humidification and lowered water consumption.

To summarize, we demonstrated that the NTs array electrode works using O_2 or Air as reactant, in spite of the absence of ionomer in its structure. So, this upsets the common representation of the electrode's operation because, in our case, there is no contact between the ionomer phase and the electrocatalyst. We have no clear explanation why the performance remains satisfactory despite this feature, but two main hypotheses can be drawn:

- Only the catalyst in close contact with the membrane area, which means directly accessible to protons, is used during operation. In that case, the actual active area would be less than measured by CV, and thus, the local surface activity of the catalyst would be even higher than what we report.
- Protons could move in hydrated state over a long range all along the tubes (200 nm). This can explain the narrower window of operation of the electrode in term of RH compared to Pt/C electrode.

Thus, efforts are still needed to understand in which extent water management in the NT array electrode is influenced by its thickness, by the presence of a dense layer between the tubes which may alter the water and proton transport, or by its peculiar nanostructure.

Work is in progress to study the durability of the NTs Array electrode as well as to improve its performance, especially at high relative humidity, by tuning its nanostructure and by adding ionomer.

4. Conclusion

A simple and reliable process to obtain MEAs based on supportless Pt NTs arrays has been successfully developed using electron beam evaporation. The process consists of only three steps, it is based on commercial AAO templates and shows high repeatability. The NTs array electrode is regular, ultrathin (< 200 nm) and includes no carbon support. The NTs array exhibits excellent catalyst surface accessibility and high Pt surface specific current density during half-cell electrochemical tests. Nevertheless its ECSA is limited (around 20 $cm^2{}_{Pt}$ $cm^{-2}{}_{geo}$) in relation to conventional Pt/C dispersions (100 $cm^2{}_{Pt}$ $cm^{-2}{}_{geo}$). During PEMFC cathode operation, NTs perform better than a Pt/C electrode provided with the same ECSA due to the absence of the porous carbon support and to the consequent catalyst accessibility and lower mass transport resistance. The NTs array MEA exhibits optimum performance at 30%RH humidification, instead of 100%RH as required by Pt/C dispersion electrodes, turning into a need for less intensive humidification when operating a PEMFC system. NTs deliver higher Pt surface specific current density than Pt/C electrodes under both dry O_2 and Air at 30%RH, while similar current density is produced under fully humidified conditions due to the onset of water management issues. The developed NTs array is a promising fuel cell electrode architecture since it allows achieving high current density per catalyst specific surface with enhanced mass transport properties. Efforts to produce nanotubes array electrodes with larger active

area by keeping low catalyst loading are foreseen in order to increase power density. Strategies consist mainly in the production of longer tubes with thinner walls, in the deposition of catalyst alloys and in the adoption of core–shell approaches [45–47].

Acknowledgements

The authors acknowledge the transversal program on New Technology for Energy of CEA and the scientific direction of CEA-Grenoble for funding this research in the frame of the NULNELEFIS project. The authors also thank Yohann Thomas for his help in obtaining the SEM cross section images shown in the supplementary information, the research and technical staff of the LCPEM Lab for the helpful support and Denis Buttard for the fruitful discussions about porous alumina.

Appendix A. Supplementary data

Supplementary material related to this article can be found, in the online version, at http://dx.doi.org/10.1016/j.apcatb.2014.09.075.

References

[1] S. Litster, G. McLean, J. Power Sources 130 (2004) 61.
[2] V. Mehta, J. Smith Cooper, J. Power Sources 114 (2003) 32.
[3] S. Mukerjee, J. Appl. Electrochem. 20 (1990) 537.
[4] K. Kinoshita, J. Electrochem. Soc. 137 (1990) 3.
[5] Y. Shao, J. Wang, R. Kou, M. Engelhard, J. Liu, Y. Wang, Y. Lin, Electrochim. Acta 54 (2009) 3109.
[6] Y. Shao, G. Yin, Y. Gao, J. Power Sources 171 (2007) 558.
[7] J. Wu, X.Z. Yuan, J.J. Martin, H. Wang, J. Zhang, J. Shen, S. Wu, W. Merida, J. Power Sources 184 (2008) 104.
[8] Y. Bultel, K. Wiezell, F. Jaouen, P. Ozil, G. Lindbergh, Electrochim. Acta 51 (2005) 474.
[9] E. Antolini, Appl. Catal. B: Environ. 100 (2010) 413–426.
[10] P. Hernández-Fernández, M. Montiela, P. Ocóna, J.L. Gómez de la Fuente, S. García-Rodríguez, S. Rojas, J.L.G. Fierro, Appl. Catal. B: Environ. 99 (2010) 343–352.
[11] S.-Y. Huang, P. Ganesan, B.N. Popov, Appl. Catal. B: Environ. 93 (2009) 75–81.
[12] S. Yin, S. Mu, H. Lv, N. Cheng, M. Pan, Z. Fu, Appl. Catal. B: Environ. 93 (2010) 233–240.
[13] D. Sebastián, A.G. Ruíz, I. Suelves, R. Moliner, M.J. Lázaro, V. Baglio, A. Stassi, A.S. Aricò, Appl. Catal. B: Environ. 115–116 (2012) 269–275.
[14] D. Sebastián, I. Suelvesa, R. Molinera, M.J. Lázaro, A. Stassi, V. Baglio, A.S. Aricò, Appl. Catal. B: Environ. 132–133 (2013) 22–27.
[15] E. Antolini, Appl. Catal. B: Environ. 74 (2007) 324–336.
[16] A. Stassi, I. Gatto, V. Baglio, E. Passalacqua, A.S. Aricò, Appl. Catal. B: Environ. 142–143 (2013) 15–24.
[17] L. Xie, P. Brault, C. Coutanceau, J.-M. Bauchire, A. Caillard, S. Baranton, J. Berndt, E.C. Neyts, Appl. Catal. B: Environ. (2015), http://dx.doi.org/10.1016/j.apcatb.2014.06.032.
[18] Y.N. Xia, P.D. Yang, Y.G. Sun, Y.Y. Wu, B. Mayers, B. Gates, Y.D. Yin, F. Kim, Y.Q. Yan, Adv. Mater. 15 (2003) 353.
[19] Y.G. Sun, B. Mayers, Y.N. Xia, Adv. Mater. 15 (2003) 641.
[20] C.M. Cobley, D.J. Campbell, Y.N. Xia, Adv. Mater. 20 (2008) 748.
[21] Y.G. Sun, Y.N. Xia, Adv. Mater. 16 (2004) 264.
[22] S.E. Skrabalak, J. Chen, L. Au, X. Lu, X. Li, Y. Xia, Adv. Mater. 19 (2007) 3177.
[23] S. Zhang, Y. Shao, G. Yina, Y. Lin, J. Mater. Chem. A 1 (2013) 4631.
[24] S.M. Alia, G. Zhang, D. Kisailus, D. Li, S. Gu, K. Jensen, Y. Yan, Adv. Funct. Mater. 20 (2010) 3742.
[25] Z. Chen, M. Waje, W. Li, Y. Yan, Angew. Chem. Int. Ed. 46 (2007) 4060.
[26] X. Zhang, D. Dong, D. Li, T. Williams, H. Wang, P.A. Webley, Electrochem. Commun. 11 (2009) 190.
[27] C.-H. Cui, S.-H. Yu, Acc. Chem. Res. 46 (2013) 1427.
[28] A.B. Papandrew, R.W. Atkinson III, G.A. Goenaga, S.S. Kocha, J.W. Zack, B.S. Pivovar, T.A. Zawodzinski Jr., J. Electrochem. Soc. 8 (160) (2013) F848.
[29] S. Ci, J. Zou, G. Zeng, S. Luo, Z. Wen, J. Mater. Chem. 22 (2) (2012) 1673.
[30] Z.Q. Tian, S.H. Lim, C.K. Poh, Z. Tang, Z. Xia, Z. Luo, P.K. Shen, D. Chua, Y.P. Feng, Z. Shen, J. Lin, Adv. Energ. Mater. 1 (2011) 1205.
[31] W. Zhang, A.I. Minett, M. Gao, J. Zhao, J.M. Razal, G.G. Wallace, T. Romeo, J. Chen, Adv. Energ. Mater. 1 (2011) 671.
[32] M. Steinhart, R.B. Wehrspohn, U. Gosele, J.H. Wendorff, Angew. Chem. Int. Ed. 43 (2004) 1334.
[33] Y. Liu, J. Goebl, Y. Yin, Chem. Soc. Rev. 42 (2013) 2610.
[34] M.D. Dickey, E.A. Weiss, E.J. Smythe, R.C. Chiechi, F. Capasso, G.M. Whitesides, ACS Nano 2 (2008) 4.
[35] J. Zhang, PEM Fuel Cell Electrocatalysts and Catalyst Layers: Fundamentals and Applications, Springer-Verlag, London, 2008.
[36] P. Fugier, S. Passot, C. Anglade, L. Guétaz, N. Guillet, E. De Vito, S. Mailley, A.A. Franco, J. Electrochem. Soc. 157 (2010) B943.
[37] F. Lazar, A. Morin, N. Pauc, P. Gentile, S. Donet, L. Guetaz, O. Sicardy, Electrochim. Acta 78 (2012) 98.
[38] S. Galbiati, A. Morin, N. Pauc, Electrochim. Acta 125 (2014) 107.
[39] F. Muench, S. Kaserer, U. Kunz, I. Svoboda, J. Brotz, S. Lauterbach, H.-J. Kleebe, C. Roth, W. Ensinger, J. Mater. Chem. 21 (2011) 6286.
[40] M. Uchida, Y.-C. Park, K. Kakinuma, H. Yano, D.A. Tryk, T. Kamino, H. Uchida, M. Watanabe, Phys. Chem. Chem. Phys. 15 (2013) 11236.
[41] T. Vidakovic, M. Christov, K. Sundmacher, Electrochim. Acta 52 (2007) 5606.
[42] A. Fischer, J. Jindra, H. Wendt, J. Appl. Electrochem. 28 (1998) 277.
[43] M.S. Wilson, S. Gottesfeld, J. Appl. Electrochem. 22 (1992) 1.
[44] C.-H. Cui, H.-H. Li, S.-H. Yu, Chem. Commun. 46 (2010) 940.
[45] H.-H. Li, C.-H. Cui, S. Zhao, H.-B. Yao, M.-R. Gao, F.-J. Fan, S.-H. Yu, Adv. Energ. Mater. 2 (2012) 1182.
[46] S.M. Alia, K. Jensen, C. Contreras, F. Garzon, B. Pivovar, Y. Yan, ACS Catal. 3 (2013) 358.
[47] L. Su, S. Shrestha, Z. Zhang, W. Mustain, Y. Lei, J. Mater. Chem. A 1 (2013) 12293.